166 (2022) 207225

Contents lists available at ScienceDirect

Micro and Nanostructures

journal homepage: www.journals.elsevier.com/micro-and-nanostructures

Linear and nonlinear optical properties of a superlattice with periodically increased well width under electric and magnetic fields

D. Altun [a,b], O. Ozturk [c], B.O. Alaydin [a,d], E. Ozturk [d,*]

[a] Nanophotonic Application and Research Center, Sivas Cumhuriyet University, 58140, Sivas, Turkiye
[b] Department of Electricity and Energy, Sivas Vocational College, Sivas Cumhuriyet University, 58140, Sivas, Turkiye
[c] Department of Nanotechnology Engineering, Engineering Faculty, Sivas Cumhuriyet University, 58140, Sivas, Turkiye
[d] Department of Physics, Science Faculty, Sivas Cumhuriyet University, 58140, Sivas, Turkiye

ARTICLE INFO

Keywords:
Superlattice
Linear and nonlinear optical properties
GaAs/$Al_xGa_{1-x}As$
Electric field
Magnetic field

ABSTRACT

In this paper, we have studied the electronic and optical properties of GaAs/$Al_xGa_{1-x}As$ superlattice with periodically increased well width. Under effective mass approximation, the finite element method is used to obtain wavefunctions and corresponding energy eigenvalues for several electric field (F) and magnetic field (B) values. We have shown that the increasing well width has a major effect on the localization of the first two energy states. The direction of the applied electric field shifts the localization position of the probability density of electrons to the left and right. For B = 0 (according to the parameters used), F = 5 kV/cm (especially for the difference between the first two energy levels (E_{12})) is a critical value. While the E_{12} value decreases in the range from −30 kV/cm to 5 kV/cm, it increases for the 5 < F < 30 kV/cm range. This behavior causes a red or blue shift in the optical spectrum. Also, F = −30 kV/cm causes more change in the structure than F = 30 kV/cm. In addition, the localization of the electrons is observed in the center of the superlattice under applied magnetic fields. The optical absorption coefficients and the refractive index changes are affected by applied F and B intensities. We can say that the electro-optical features of the superlattice have changed significantly with the combined effect of F and B values. This is desired for semiconductor optical device applications to have stable performances.

1. Introduction

Research about nanoscale devices and structures is one of the popular fields of science due to being the basis of important applications in the field of automotive, medical, and security. In the current technology, major nanoscale devices are composed of quantum wells (QWs) so studies about QWs are still going on to improve current device performances. In addition to QWs, superlattices which are cascaded QWs are also taken attention due to superior optical and electrical properties [1,2]. QWs have been extensively analyzed in the literature by considering the interband and intersubband transitions [3–5]. Different potential shapes were mainly considered. Interband absorption in square and semi-parabolic near-surface QWs was analyzed under an intense laser field by Niculescu and Eseanu [6]. The nonlinear optical rectification, the second harmonic generation, and the third harmonic generation

* Corresponding author.
E-mail address: eozturk@cumhuriyet.edu.tr (E. Ozturk).

https://doi.org/10.1016/j.micrna.2022.207225
Received 11 February 2022; Received in revised form 4 April 2022; Accepted 5 April 2022
Available online 14 April 2022

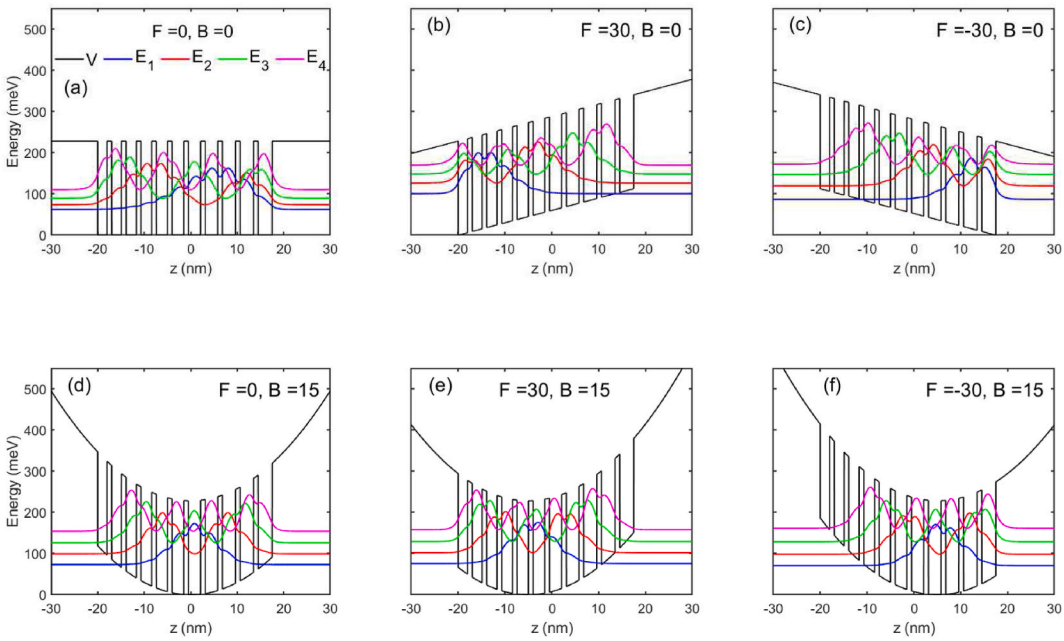

Fig. 1. The potential profiles and the first four electron energy levels corresponding to the associated PDWs for a) F = 0; B = 0, b) F = 30 kV/cm; B = 0, c) F = −30 kV/cm; B = 0, d) F = 0; B = 15 T, e) F = 30 kV/cm; B = 15T and f) F = −30 kV/cm; B = 15T.

coefficients were examined for different potential profiles [7,8]. Asymmetric GaAs n-type delta-doped potentials were considered by Rodríguez-Magdaleno et al. [9]. Keshavarz and Karimi studied the intersubband optical absorption coefficients (OACs) in symmetric double semi-parabolic QWs [10], and the second harmonic generation in asymmetric double semi-parabolic QWs [11]. The laser, electric, and magnetic fields were used in most of the studies to simulate the electronics and optical properties of the QWs [12–16]. The linear and nonlinear optical properties of multiple-step QWs under the laser, electric, and magnetic fields were analyzed by Restrepo et al. [17]. As a different material structure, second-order nonlinear optical properties for InGaN/AlGaN QW under the intense laser field were studied by Karimi and Vafaei [18]. Transport properties of the two-dimensional electron gas in wide AlP QWs including temperature and correlation effects were considered by Tai and Khanh [19]. Experimentally, intersubband transitions in pseudomorphic InGaAs/GaAs/AlGaAs multiple-step QWs were studied by Li et al. [20]. Nonlinear optical rectification in semi-parabolic QWs under applied electric field was deeply investigated by Karabulut and Safak [21]. Zhang worked on the electric field effect on the intersubband refractive index changes (RICs) in asymmetrical semi parabolic and symmetrical parabolic QWs [22]. Baskoutas et al. made a major contribution to the literature for inverse parabolic QWs by investigating the OACs under static external electric fields [23]. A redshift is an increase in the wavelength, and a corresponding decrease in the frequency and photon energy, of electromagnetic radiation (such as light). The opposite change, a decrease in wavelength and simultaneous increase in frequency and energy, is known as a blue shift. Ozturk et al. calculated the intense laser field effect on the nonlinear optical properties of triple quantum wells consisting of parabolic and inverse-parabolic QWs [24]. The authors showed that the spectrum of the resonance peak varies depending on the laser field of the red or blue shift. Although such a broad literature about QWs, theoretical studies about the linear and nonlinear optical properties of the superlattices are limited [25,26] and further studies are needed. In the quantum cascade laser structures, the laser's active region contains quantum wells (injector and radiative wells) around 8–13 [1,27–29]. Furthermore, Donchev et al. examined the luminescence properties of a superlattice consisting of eleven quantum wells in the case of zero external fields [28]. The parameters in this study are different from Ref. [28] and external fields are applied to this structure.

In the current paper, we have studied the superlattice with periodically increased well width (WW) on the optical properties under applied electric and magnetic fields. The linear absorption coefficients (LACs), nonlinear absorption coefficients (NACs), total absorption coefficients (TACs), linear refractive index change (LRIC), nonlinear refractive index change (NRIC), and total refractive index change (TRIC) are calculated dependent on these external field values. To the best of our knowledge, this is the first research paper to study the optical properties of a superlattice with different WWs. We organize the paper as follows; theory and method are given in section 2. Section 3 presents the novel results and discussion. We finish the paper with a conclusion, which is given in section 4.

2. Theory and method

The finite element method is used to obtain the wave functions (WFs) and corresponding energy levels (ELs) under effective mass approximation. In matrix formalism, time-independent Hamiltonian of the GaAs/$Al_xGa_{1-x}As$ superlattice with periodically increased WW is given in Equation (1),

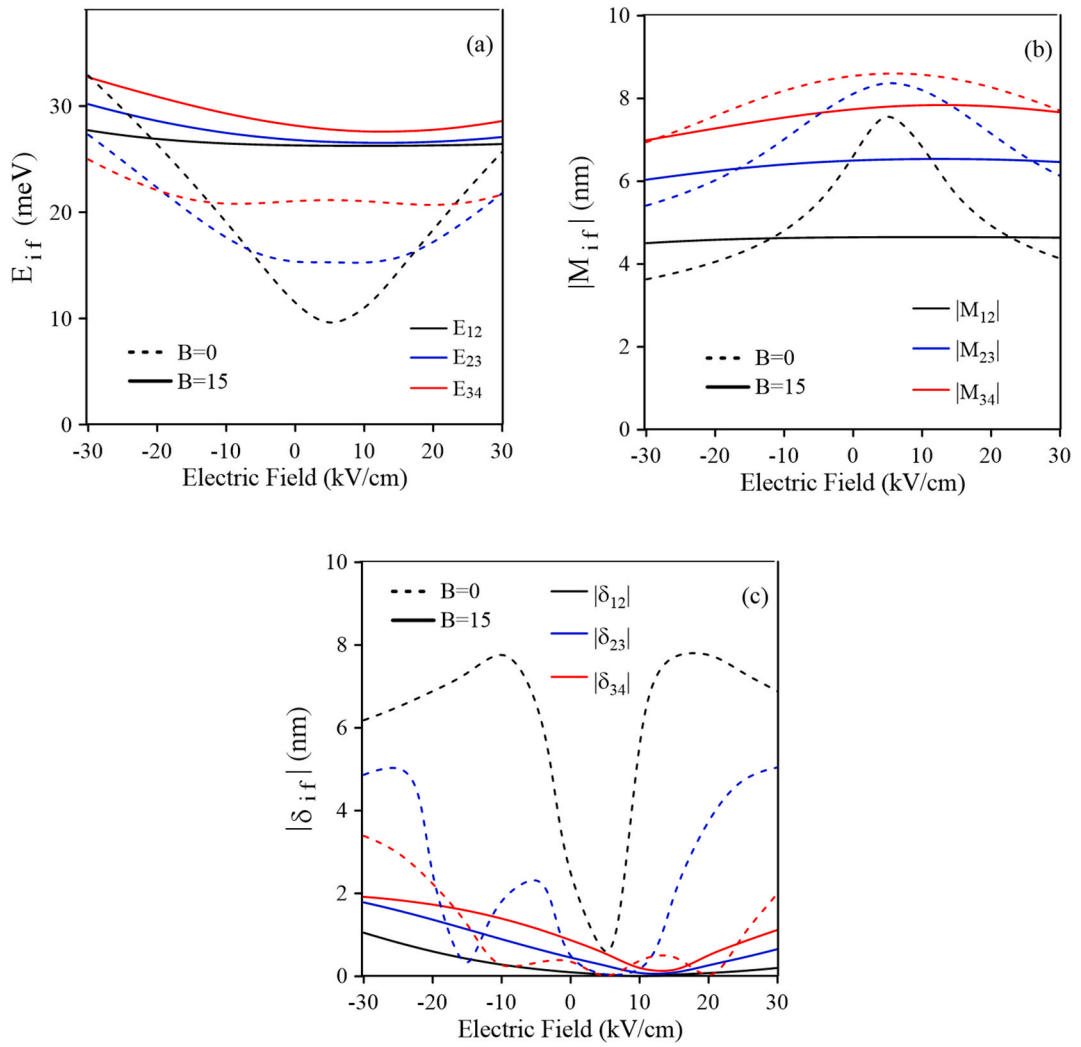

Fig. 2. For different B values a) several energy differences, b) several ISB DMME, c) several intrasubband DMME values as a function of the electric field.

Table 1
The energy differences and the RP values of LACs for different F and B values.

B (T)	F (kV/cm)	E_{12} (meV)	E_{23} (meV)	E_{34} (meV)	β^{12}_{max} (1/cm)	β^{23}_{max} (1/cm)	β^{34}_{max} (1/cm)
0	0	11.5	15.3	21.0	1219	2453	3733
	30	25.7	21.8	21.7	1067	1991	3127
	−30	32.9	27.3	24.9	1053	1943	2927
15	0	26.3	26.8	28.2	1379	2751	4096
	30	26.4	27.1	28.6	1380	2750	4081
	−30	27.7	30.2	32.7	1366	2672	3883

$$H = -\frac{\hbar^2}{2m^*}\frac{d^2}{dz^2} + \frac{e^2\ B^2\ z^2}{2\ m^* c^2} + e\ F\ z + V(z) \tag{1}$$

where the second-order differential is defined as (details of the diagonalization method are found in Ref. [30]).

$$\frac{d^2}{dz^2} = [-2\ \ \mathrm{diag}(\mathrm{ones}(1, N_z)) + \ \ \mathrm{diag}(\mathrm{ones}(1, N_z - 1), -1) + \mathrm{diag}(\mathrm{ones}(1, N_z - 1), 1)]^2 \tag{2}$$

where m^* describes the effective mass of the electron, it is taken as 0.067 m_0 due to lattice matching between GaAs and $Al_xGa_{1-x}As$ (m_0

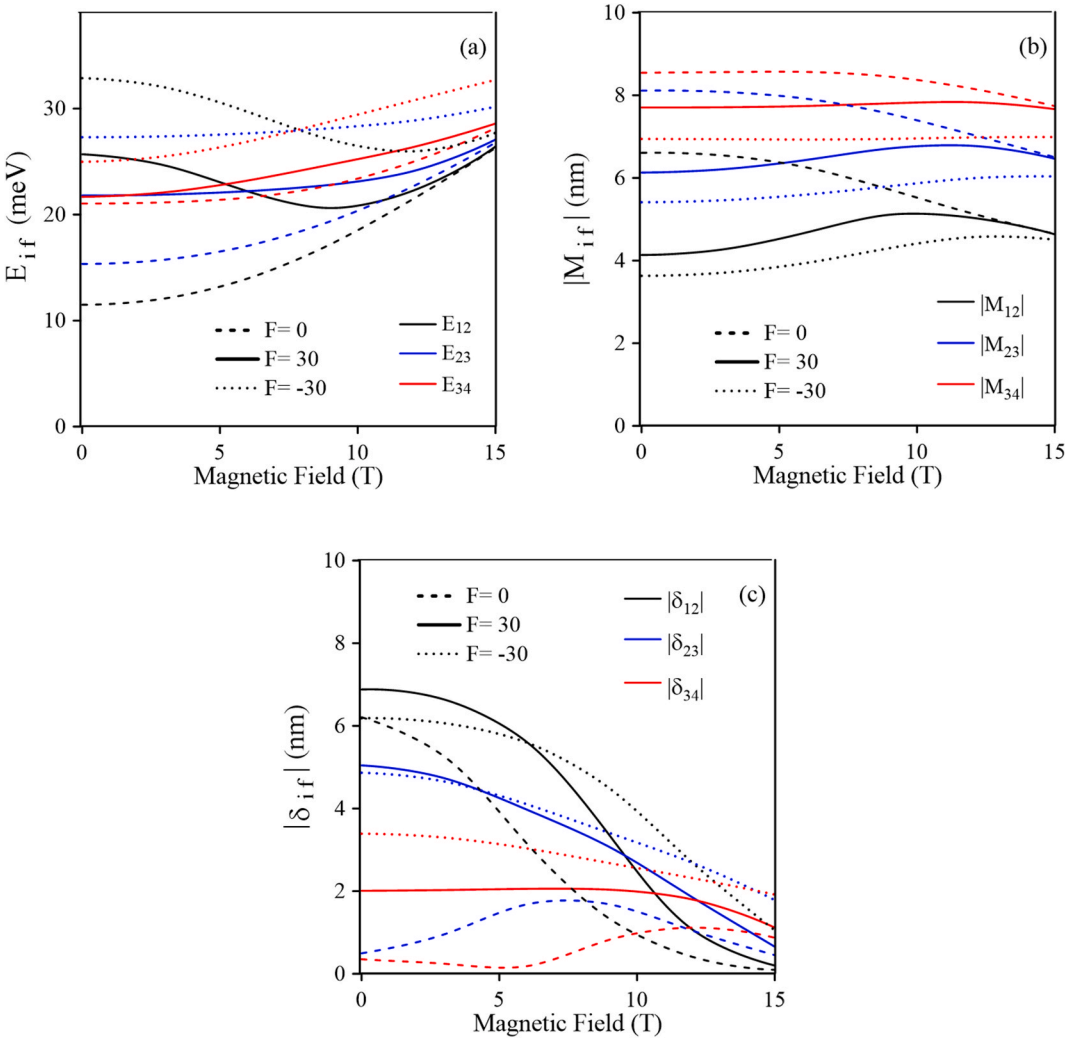

Fig. 3. For different F values a) several energy differences, b) several ISB DMME, c) several intrasubband DMME values as a function of the magnetic field.

is the free electron mass), e is the electron charge, N_z is the length of the matrix to define the total quantum region, F is the electric field in the growth direction, B is the magnetic field applied perpendicular to the growth direction, and V(z) is the confinement potential. For the superlattice formed with eleven wells, the leftmost WW is 2 nm, and the rightmost WW is 3 nm by increasing 0.1 nm to the right. Barrier widths are 1 nm and kept constant. For GaAs/$Al_xGa_{1-x}As$ superlattice, V_0 is the band discontinuity and calculated by $V_0 = Q_c(1155\ x + 370\ x^2)$meV, where $Q_c = \frac{\Delta E_c}{\Delta E_g} = 0.6$ is the conduction band offset parameter (where $\Delta E_g = \Delta E_c + \Delta E_v$, E_c and ΔE_v are the conduction and valence band discontinuities) and x is the Al concentration in the barrier regions (for $x = 0.3$, $V_0 = 228$ meV) [11,31].

To solve Equation (1), the diagonalization method is used in one dimension. After obtaining the ELs and their corresponding electron WFs, LACs, third-order NACs, and TACs for intersubband (ISB) transitions for the first four ELs can easily be given using the density matrix approach as [32], respectively.

$$\beta_{if}^{(1)}(\omega) = \omega\sqrt{\frac{\mu}{\varepsilon_r}}|M_{if}|^2 \frac{e^2\sigma_v\hbar\ \Gamma}{(E_{if} - \hbar\omega)^2 + (\hbar\ \Gamma)^2} \tag{3}$$

$$\beta_{if}^{(3)}(\omega, I) = -2\omega\sqrt{\frac{\mu}{\varepsilon_r}}|M_{if}|^4 \left(\frac{I}{\varepsilon_0 c\ n_r}\right) \frac{e^4\sigma_v\hbar\ \Gamma}{\left\{(E_{if} - \hbar\omega)^2 + (\hbar\ \Gamma)^2\right\}^2} \times \left[1 - \frac{|\delta_{if}|^2}{|2M_{if}|^2}\left(\frac{(E_{if} - \hbar\omega)^2 - (\hbar\ \Gamma)^2 + 2E_{if}(E_{if} - \hbar\omega)}{(E_{if})^2 + (\hbar\ \Gamma)^2}\right)\right] \tag{4}$$

$$\beta_{if}(\omega, I) = \beta_{if}^{(1)}(\omega) + \beta_{if}^{(3)}(\omega, I) \tag{5}$$

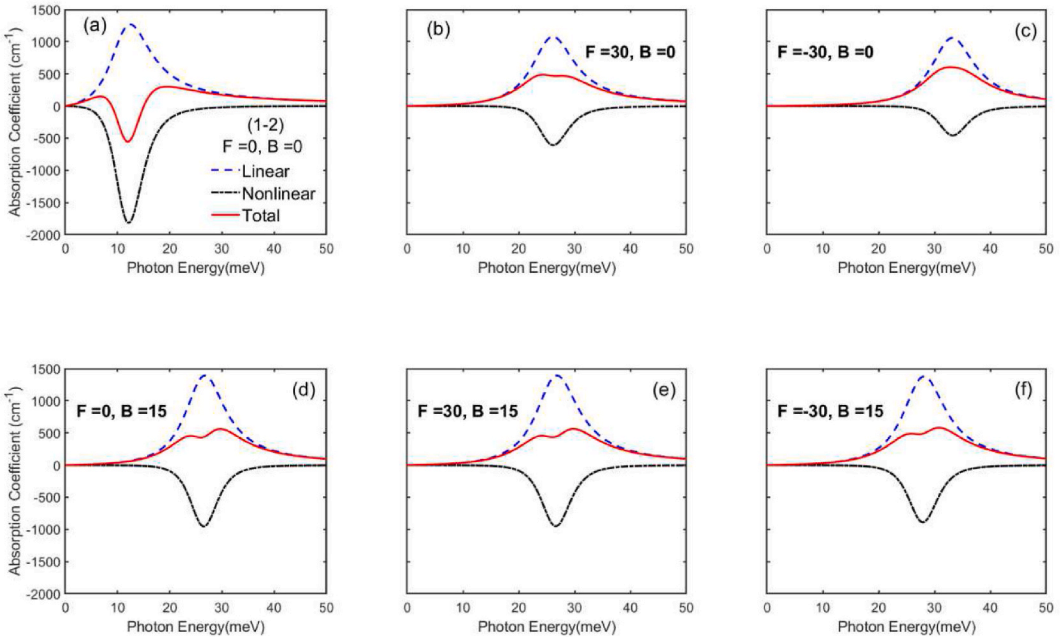

Fig. 4. The variation of the OACs as a function of the photon energy for a) F = 0; B = 0, b) F = 30 kV/cm; B = 0, c) F = −30 kV/cm; B = 0, d) F = 0; B = 15 T, e) F = 30 kV/cm; B = 15T and f) F = −30 kV/cm; B = 15T for (1–2) transition. (I = 0.3 MW/cm^2).

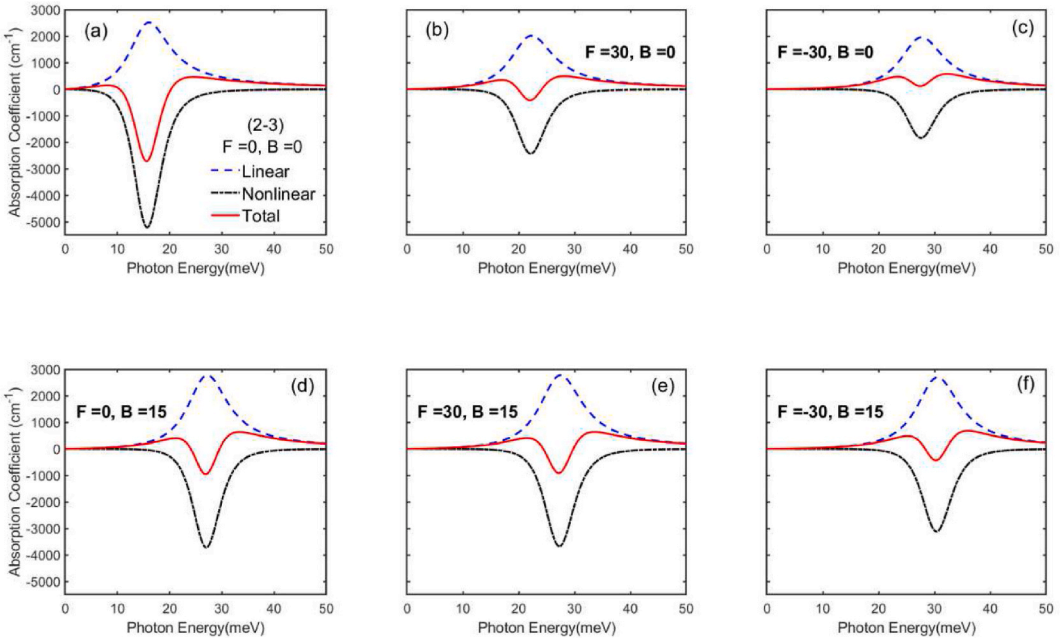

Fig. 5. For the (2–3) transition, same as Fig. 4 description.

The LRICs, NRICs, and TRICs can be derived as [33], respectively.

$$\frac{\Delta n_{if}^{(1)}(\omega)}{n_r} = \frac{e^2\sigma_v}{2\varepsilon_0 n_r^2}|M_{if}|^2 \frac{(E_{if} - \hbar\omega)}{(E_{if} - \hbar\omega)^2 + (\hbar\ \Gamma)^2} \tag{6}$$

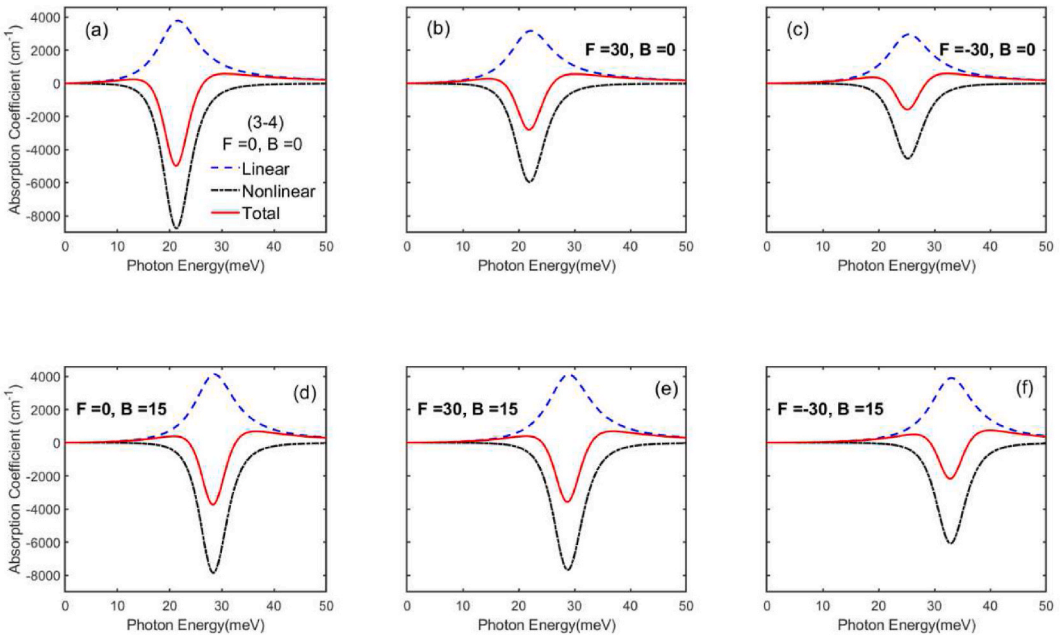

Fig. 6. For the (3–4) transition, same as Fig. 4 description.

$$\frac{\Delta n_{if}^{(3)}(\omega, I)}{n_r} = -\frac{\mu\ c}{4\mathscr{E}_0 n_r^3}\left|M_{if}\right|^2 \frac{e^4\sigma_v\ I}{\left\{\left(E_{if}-\hbar\omega\right)^2+\left(\hbar\ \Gamma\right)^2\right\}^2}$$
$$\times\left[4\left(E_{if}-\hbar\omega\right)\left|M_{if}\right|^2-\frac{\delta_{if}{}^2}{\left(E_{if}\right)^2+\left(\hbar\ \Gamma\right)^2}\times\left\{\left(E_{if}-\hbar\omega\right)\left[E_{if}\ \left(E_{if}-\hbar\omega\right)-\left(\hbar\ \Gamma\right)^2\right]-\left(\hbar\ \Gamma\right)^2\left[2E_{if}-\hbar\omega\right]\right\}\right] \tag{7}$$

$$\frac{\Delta n_{if}(\omega, I)}{n_r} = \frac{\Delta n_{if}^{(1)}(\omega)}{n_r} + \frac{\Delta n_{if}^{(3)}(\omega, I)}{n_r} \tag{8}$$

In particular, we have investigated the resonance peaks (RPs) of LACs in this study [5],

$$\beta_{max}^{if}\left(\omega=\omega_{if},\ \ I=0\right) = \left|M_{if}\right|^2 \frac{e^2\sigma_v\omega_{if}\ \ T}{\hbar\mathscr{E}_0\ \ c\ \ n_r} \tag{9}$$

and ISB dipole moment matrix elements (DMMEs) are defined by

$$M_{if} = \int \Psi_f^*\ \ z\ \ \Psi_i\ \ dz\ \ ,(i,f=1,2,3,4) \tag{10}$$

Here, $\delta_{if} = M_{ff} - M_{ii}$ is the intrasubband DMMEs, I is the optical light intensity, ω is the angular frequency of the incident photon, ($E_{if} = E_f - E_i = \hbar\omega_{if}$), E_f and E_i represent the quantized ELs for the last and first states, $\mathscr{E}_0$ is the vacuum permittivity, $\mathscr{E}_r$ is the real part of the permittivity, μ is the magnetic permeability , n_r is the refractive index, σ_v is the carrier density.

3. Result and discussion

With and without F and B, we have theoretically investigated the electronic and optical features for the (1–2), (2–3), and (3–4) transitions in the superlattice. (Other transitions ((1–3), (1–4), and (2–4)) are not included in the study because of negligibly small values). In this study, we have taken $\sigma_v = 4x10^{16}cm^{-3}$ $T = 1/\Gamma = 0.14$ ps [11,32], and I are respectively 0.1, 0.3, and 0.5MW/ cm^2. The electric field values in the legends of all figures are in kV/cm, and the magnetic field values are in T.

In the superlattice, which consists of eleven wells, the comments will be made by numbering the wells from left to right. Without and with F and B, Fig. 1(a–f) shows the potential profile, the first four bounded ELs, and the associated probability densities (PDs) for superlattice. By increasing WW, the ELs and the PDs of the electrons in the superlattice have changed significantly. E_1 and E_2 ELs are mostly affected by the change of WW. Since WWs are not symmetrical, without external fields the electrons in the E_1 level are localized in the eighth and ninth wells and are not exist in the first three wells due to narrow WWs. The electrons in the E_2 level are mostly in the fourth, fifth, and tenth wells. The electrons in the excited states are distributed throughout the entire superlattice region as they are more energetic than the first two ELs (Fig. 1a). Since the structure is tilted to the left for F = 30 kV/cm, the PD of the electrons in E_1 EL

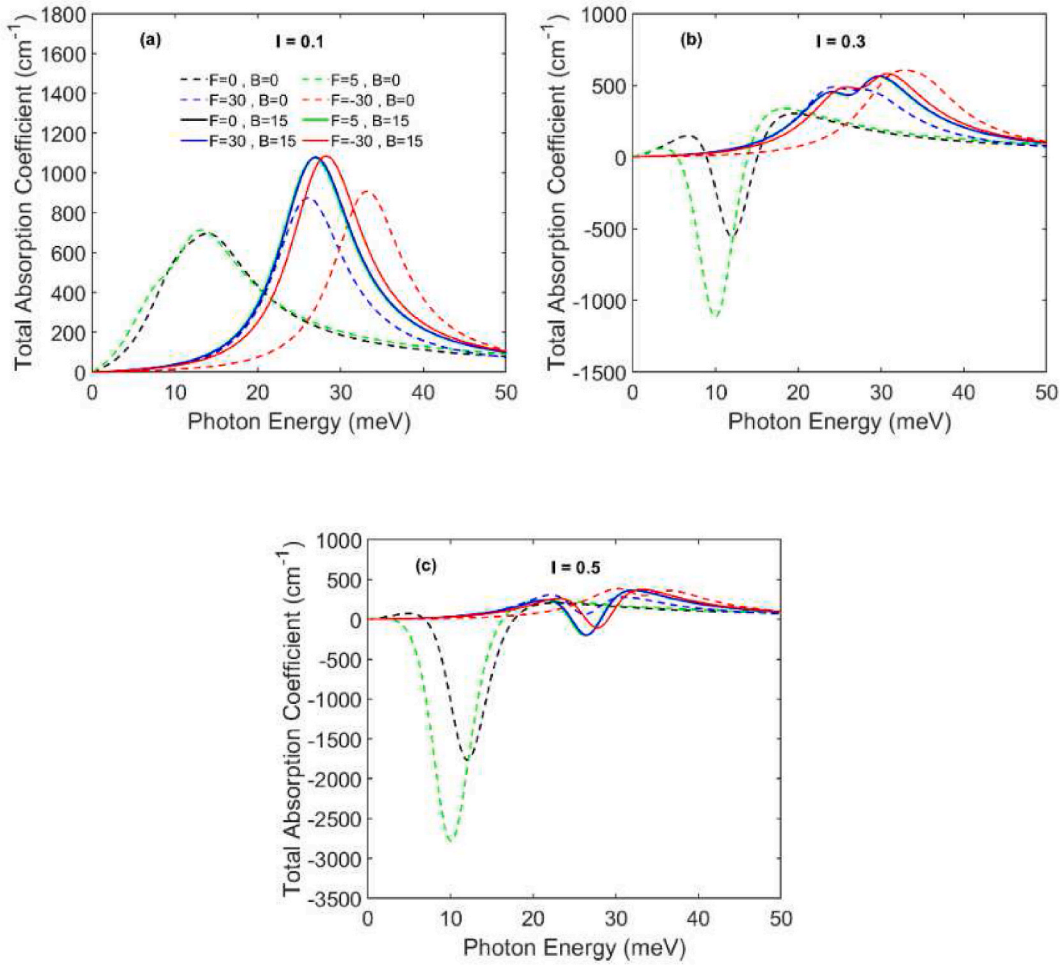

Fig. 7. TAC of (1-2) transitions versus the photon energy for a) I = 0.1, b) 0.3, and c) 0.5 MW/cm^2 for four F and two B values.

is more on the left side, and EL is more on the middle side. However, E_3 and E_4 localize in the wells to the right of the superlattice due to wider WWs (Fig. 1b). The superlattice is tilted to the right because of the negatively applied F, and the ELs vary depending on the shape of the potential, and the electrons in E_1 EL shift to the left as expected (Fig. 1c). In addition, the ELs obtained for F = 30 kV/cm are higher than those for both F = 0 and F = −30 kV/cm because narrower wells on the left side of the superlattice, which shifts ELs to upper energies. The magnetic field effect is very different from the electric field. As the magnetic field is applied, the ELs localize in the center of the superlattice because of the magnetic field, which changes both the depth and shape of the confinement potential (see Fig. 1(d-f)) by bending the edge of the quantum barrier at both sides of the superlattice. Furthermore, the localization of the electron for each EL becomes more homogeneous even though the thickness of the WW increases. The electron WF interaction between adjacent QWs becomes increasingly stronger with applied B, which causes more carriers to be localized in the middle of the superlattice. In this case, because of the strong coupling between QWs, ELs are pushed upwards and are higher than with B = 0 (Fig. 1d). With the combined effect of both ± F and B, both the potential profile is tilted and the geometric confinement of the carriers is varied. These effects are important for the linear and nonlinear optical response of the system. Thus, it can say that the size of both F and B affect the confinement and localization.

Three energy differences and the DMMEs values as a function of F are given in Fig. 2 for different B values. At the same time, the energy differences for different F and B values are given in Table 1. F = 5 kV/cm (especially for E_{12}) is a critical value (according to the parameters used) for B = 0. The E_{12} decreases in the range from −30 kV/cm to 5 kV/cm, but rises for 5 < F < 30 kV/cm range. The E_{12} values are 15.12, 11.49, and 9.61 meV for F = −5, 0, and 5 kV/cm, seriatim. This behavior causes a red or blue shift in linear and nonlinear transitions. The value of E_{34} varies less than E_{12} and E_{23}. For B = 15T, less variation is seen in the energy differences drawn against the electric field. Similar situations are seen for the DMMEs in Fig. 2b. The PD related to the first four-electron ELs are important for the values of DMMEs. The overlap between the first four bound state WFs varies due to the tilt and bending of the superlattice potential profile with F and B values. These effects on the DMMEs are related to the behavior of electron WFs in the superlattice. As seen in Fig. 2 (b, c), the DMMEs change with varying F and B owing to the overlap between the first four states WFs. Since the localization of WFs in all superlattice modifies, the alterations of the ISB and intrasubband DMMEs are different from each

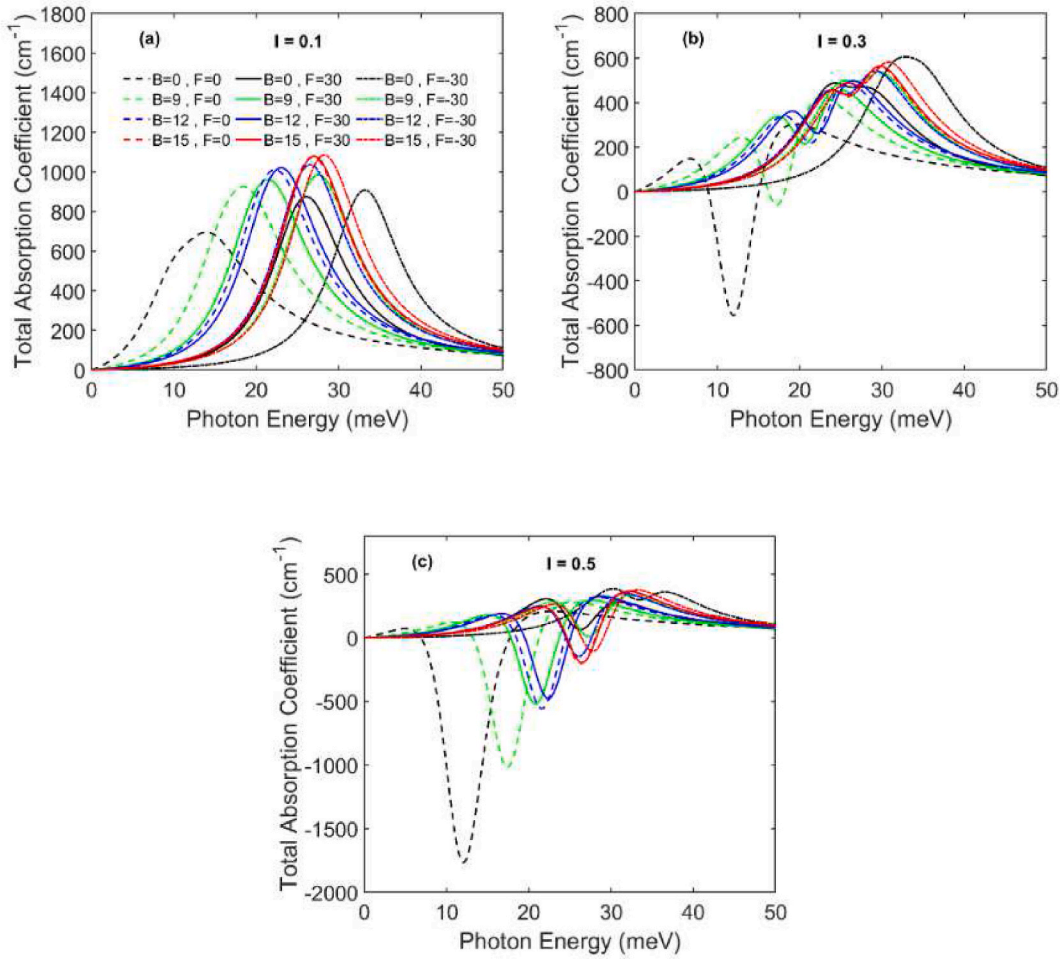

Fig. 8. TAC of (1-2) transitions as a function of the photon energy for a) I = 0.1, b) 0.3, and c) 0.5 MW/cm^2 for four B and three F values.

other. Such a dependence of the F and B intensities on the energy differences and DMMEs could be very advantageous for a variety of potential devices.

In Fig. 3, we have shown three energy differences and several DMMEs depending on B values for three F intensities. All values are affected by the changing superlattice profile in case of simultaneously varying F and B parameters, and these values are important for the electronic and optical properties of these configurations. For F = 0, all E_{if} values are shifted upwards, with B rising due to the central localization of electrons as a result of increasing confinement. The E_{12} value, which changes against B, is affected differently by + F and –F. For F = 30 kV/cm (for F = −30 kV/cm), the E_{12} decreases up to B = 9T (B = 12T) and increases after this value. The absorption spectrum shows blue or redshifts depending on F and B sizes. The energy differences at F = −30 kV/cm are larger than at F = 0 and F = 30 kV/cm. This situation is quite evident in Figs. 2a and 3a. Expressions described for E_{if} values in Fig. 3a, also apply to ISB DMMEs in Fig. 3b. The intrasubband DMMEs are connected to both F and B.

For different F and B values, Fig. 4, Fig. 5, and Fig. 6 show the modification of the LACs, NACs, and TACs versus the incident photon energy for (1–2), (2–3), and (3–4) transitions, seriatim. These coefficients vary in magnitude and energy range for different F and B values. TAC decreases by the negative NAC additive in the existence incident optical intensity. The RP of TAC may be bleached at enough optical densities. This branching is because of the adding of the third-order nonlinear term. For (1–2), (2–3), and (3–4) transitions, the RPs of TOAC are branching for F = 0 and B = 0. While there is no branching at the transition (1–2) with increasing F and B magnitudes, the branching is still present at the transitions (2–3 and (3–4), and less for F = −30 kV/cm and B = 0. For B = 0, both LAC and NAC values at F = 0 are greater than at both F = 30 and F = −30 kV/cm for (1–2) transition. Therefore, TOAC has both negative values and large branching. For B = 15T, similar behavior is seen at all F values. If we keep the electric field constant and look at the incremental change of the magnetic field from B = 0–15T; i) For F = 0, LAC is increasing but NAC is decreasing, so TAC gives smaller branching. ii) For F = 30 kV/cm, both LAC and NAC increase, TAC still has little branching. iii) For F = −30 kV/cm, both LAC and NAC increased, TAC now starts to give slight branching. The detailed variations of the absorption spectrum of TAC for transition (1–2) will be described in Fig. 7 and Fig. 8. Respectively, the peaks of LAC and NAC for the (2–3) transition are ~2 and ~3 times higher than (1–2) transition due to different DMMEs in the case of zero external fields. For (2–3) transition, the TAC has branching at all F and

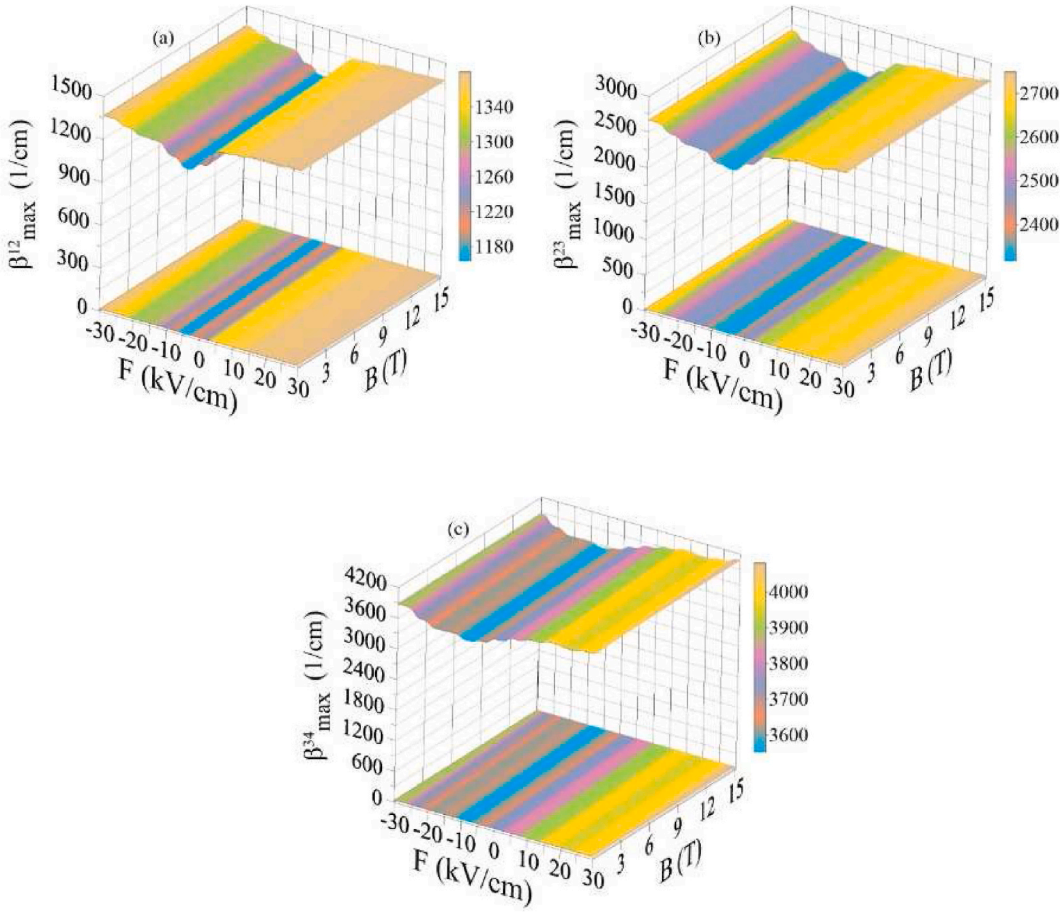

Fig. 9. RP of LACs for a) (1–2), b) (2–3), c) (3–4) transitions as a function of F (x-axis) and B (y-axis).

B intensities and is only positive for F = −30 kV/cm and B = 0. Again, the largest LAC and NAC values are provided for F = 0 and B = 0. As can be seen from the energy differences in Table 1, if F = 0 is taken as a base; when the electric field intensities are set to both F = 30 kV/cm and F = −30 kV/cm; i) in the absence of B, the absorption spectrum is blue shifted. ii) When B = 15 T, there is still a little blue shift. If B = 0 is taken as a base; in the absence and presence of F, the spectrum moves towards a blue shift with the increase of B. The (3–4) transition is affected by the F and B values, similar to the (2–3) transition. At all F and B intensities, TAC has both branching and negative values. The amount of blue shift of the absorption spectrum is different.

Since the (1–2) transition is most affected by the change of the potential profile depending on the F and B intensities, the absorption spectrum has been investigated in detail. Fig. 7(a–c) shows the TACs of (1-2) transition as a function of the photon energy for I = 0.1, 0.3, and 0.5 MW/cm^2 for four F and two B values. If F = 0 is taken as a reference point; in the absence of B, the absorption spectrum gives a redshift for F = 5 kV/cm, while it goes towards blue shift at other F values. When B = 15 T is applied, TAC is at the same location and same magnitude at F = 0, 5, and 30 kV/cm, but shows a little blue shift when only F = −30 kV/cm is applied. Since the intensity of I = 0.1 MW/cm^2 changes NAC quantitatively less than the intensities of 0.3 and 0.5 MW/cm^2, TAC is positive, high, and shows almost no branching. When I = 0.3 MW/cm^2 intensity is applied, while for B = 0 the TAC has negative values only at F = 0 and 5 kV/cm, it is positive at F = 30 and −30 kV/cm and no branching. When the optical light intensity is set to 0.3 MW/cm^2 intensity, TAC has negative values only for F = 0 and 5 kV/cm in the absence of B and TAC is positive at F = 30 and −30 kV/cm and has no branching. TAC is almost in the same position and has the same size at all values of F for B = 15 T and branching is seen. If the light intensity is set to 0.5 MW/cm^2, TAC does not have a negative value only for B = 0 and F = −30 kV/cm, it has negative values in all other F and B values, and the branching is quite evident. It can be seen from here that the value of F = −30 kV/cm creates more change in the structure than the magnitude of F = 30 kV/cm.

For four B and three F values, the TACs of (1-2) transition versus the photon energy are given in Fig. 8 (a, b, and c) for I = 0.1, 0.3, and 0.5 MW/cm^2, separately. For zero electric field intensity, the spectrum of TAC shows a blue shift for all incremental values of B. When F = 30 kV/cm is applied, it shows a redshift up to B = 9T, while it indicates a blue shift for greater than 9T. Similarly, for F = −30 kV/cm, it displays a redshift up to B = 12T, while it represents a blue shift for greater than 12T. For all F and B values, all TACs are positive, large, and unbranched for intensity I = 0.1 MW/cm^2. For I = 0.3 MW/cm^2, the TAC quantity is negative at B = 0 and 9T in the absence of F. Also, there is no branching of TAC only for F = −30 kV/cm and B = 0. At I = 0.5 MW/cm^2, the TAC has no negative value

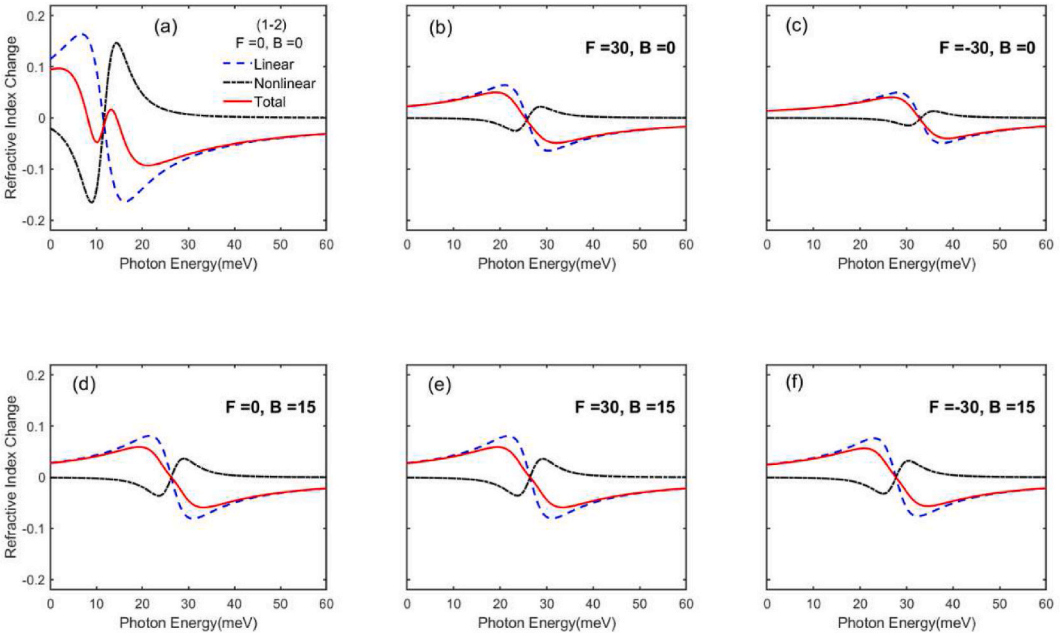

Fig. 10. The variation of the RICs as a function of the photon energy for a) F = 0; B = 0, b) F = 30 kV/cm; B = 0, c) F = −30 kV/cm; B = 0, d) F = 0; B = 15 T, e) F = 30 kV/cm; B = 15T and f) F = −30 kV/cm; B = 15T for (1–2) transition. (I = 0.3 MW/cm^2).

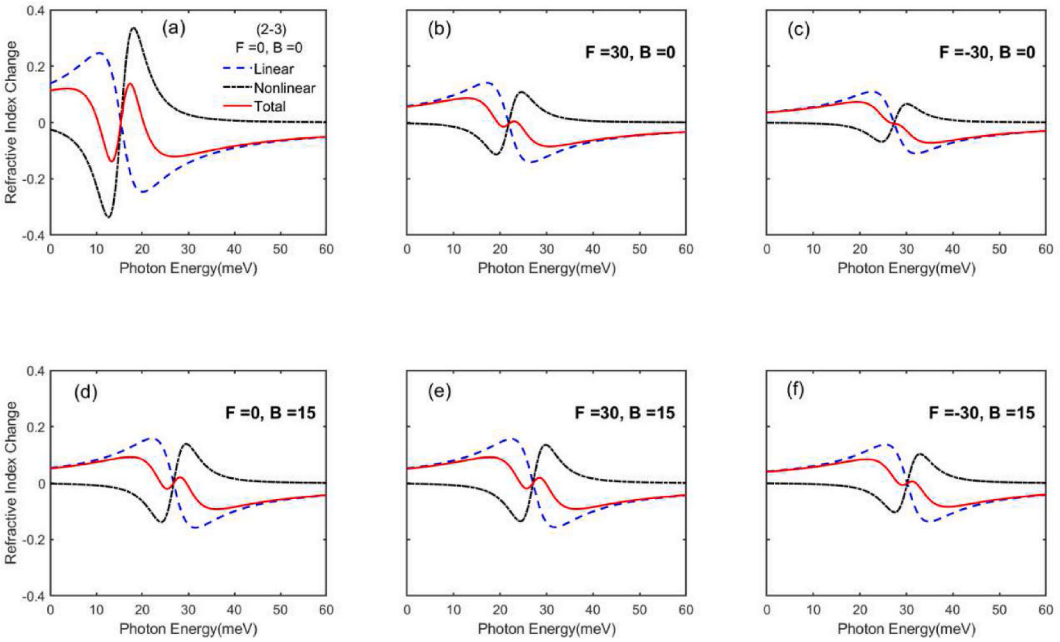

Fig. 11. For the (2–3) transition, same as Fig. 10 description.

and little branching only in the magnitudes of B = 0 and F = −30 kV/cm. TAC has negatives in all other F and B values, and the branching is quite pronounced. We can say that the structure of superlattices changes considerably with the combined effect of F and B values.

The RP of LAC for (1–2), (2–3), and (3–4) optical transitions versus both F and B parameters are shown in Fig. 9, and the color scale has also reflected the base to scale the changes. For different F and B values, these peaks are also given in Table 1. The RP of LACs for (1–2) transition is lower than (2–3) and (3–4) transition. As seen in Eq. (8), these peaks are dependent on both E_{if} difference and ISB DMME. The size and shape of the RP variation with varying F are different for rising B values.

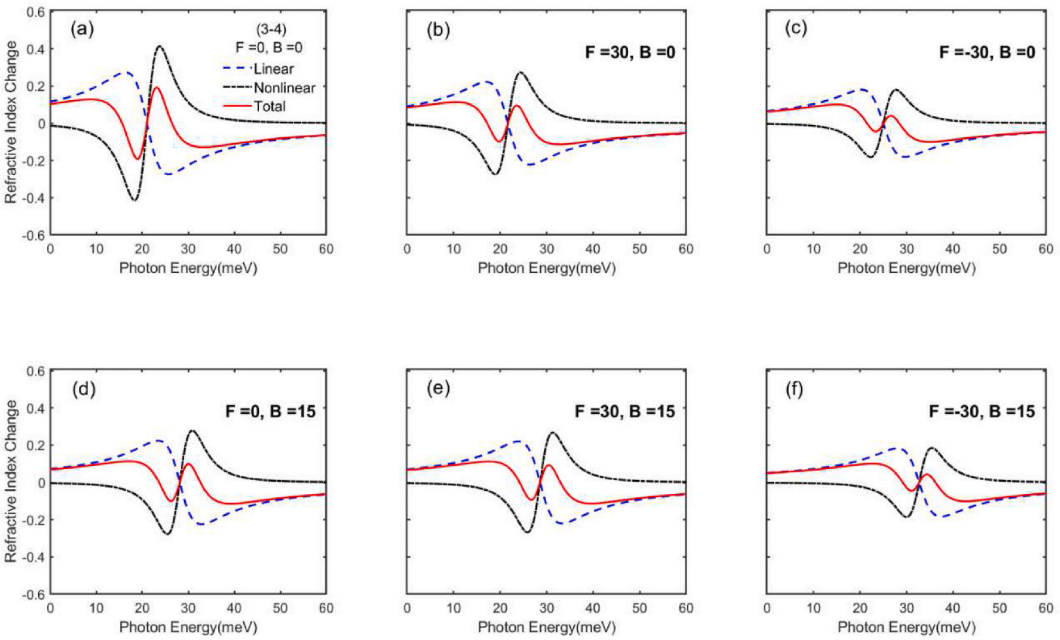

Fig. 12. For the (3–4) transition, same as Fig. 10 description.

With and without F and B, the RICs as a function of the photon energy for the (1–2), (2–3), and (3–4) transitions are shown in Fig. (10)–(12), respectively. Because the LRIC and NRIC terms are opposite in sign, any increase in the magnitude of the NRIC term will also increase the difference between them, so reduce the TRIC. All RICs are affected by all F and B intensities in a similar way to the OACs. It can say that the RICs are related to both ± F and B, and the shape of potential. For transition (3–4), all RIC values are greater than both (1–2) and (2–3) transitions, for the same intensities F and B. The main reason for these differences is due to the change in the DMMEs and the energy interval of the electronic states between which optical transition occurs.

4. Conclusion

As a conclusion, we have studied the electro-optical properties of GaAs/$Al_xGa_{1-x}As$ superlattice with periodically increased well width under applied electric and magnetic fields. The first four bounded energy levels for (1–2), (2–3), and (3–4) intrasubband transitions are considered. E_1 and E_2 ELs are mostly affected by the change of WW, while E_3 and E_4 ELs are less affected as they are more energetic. The electric field shifts the localization position of the probability density of electrons to the left and right for 30 kV/cm and −30 kV/cm, respectively. In addition, this localization is observed in the center of the superlattice under applied magnetic fields due to increased confinement and bending of the potential profile. F = 5 kV/cm value is critical for E_{12} transition energy, it is possible to tune the transition energy of the structures with the electric field. Both OACs and RICs are affected by all F and B intensities, and these are related to both ± F and B, and the shape of potential. In addition, all OAC and RIC values for (1–2) transition are lower than both (2–3) and (3–4) transitions, for the same intensities F and B. As a last, we believe that the current study can contribute design and research of superlattice-based semiconductor devices such as photodetectors and lasers by showing the way how to change optical properties.

Author contribution statement

D. Altun contributed to the introduction, data acquisition, graphic drawings, and article writing. O. Ozturk made corrections and re-modified the manuscript in the present form. B.O. Alaydin contributed with the introduction, theory and results, and discussion. E. Ozturk contributed throughout the manuscript.

Declaration of competing interest

The authors declare that they have no known competing financial interests or personal relationships that could have appeared to influence the work reported in this paper.

References

[1] C. Sirtori, P. Kruck, S. Barbieri, P. Collot, J. Nagle, M. Beck, J. Faist, U. Oesterle, GaAs/$Al_xGa_{1-x}As$ quantum cascade lasers, Appl. Phys. Lett. 73 (1998) 3486–3488.
[2] Y. Wei, A. Gin, M. Razeghi, G.J. Brown, Advanced InAs/GaSb superlattice photovoltaic detectors for very long wavelength infrared applications, Appl. Phys. Lett. 80 (2002) 3262–3264.
[3] B.O. Alaydin, E. Ozturk, S. Elagoz, Interband transitions dependent on indium concentration in $Ga_{1-x}In_xAs$/GaAs asymmetric triple quantum wells, Int. J. Mod. Phys. B 32 (2018) 1850052.
[4] O. Ozturk, E. Ozturk, S. Elagoz, The effect of intense laser field on the nonlinear optical features in asymmetric multiple step and inverse V-shaped multiple step quantum wells, Laser Phys. 29 (2019) 105401.
[5] O. Ozturk, E. Ozturk, S. Elagoz, Dependence on well widths of total optical absorption coefficient of asymmetric triple GaAlAs/GaAs and GaInAs/GaAs quantum wells, Int. J. Mod. Phys. B 33 (2019) 1950175.
[6] E.C. Niculescu, N. Eseanu, Interband absorption in square and semiparabolic near-surface quantum wells under intense laser field, Eur. Phys. J. B 79 (2011) 313–319.
[7] I. Altuntas, Effects of applied external fields on the nonlinear optical rectification, second, and third harmonic generation in a quantum well with exponentially confinement potential, Eur. Phys. J. B 94 (2021) 177.
[8] S. Şakiroğlu, F. Ungan, U. Yesilgul, M.E. Mora-Ramos, C.A. Duque, E. Kasapoglu, H. Sari, İ. Sökmen, Nonlinear optical rectification and the second and third harmonic generation in Pöschl–Teller quantum well under the intense laser field, Phys. Lett. 376 (2012) 1875–1880.
[9] K.A. Rodríguez-Magdaleno, J.C. Martínez-Orozco, I. Rodríguez-Vargas, M.E. Mora-Ramos, C.A. Duque, Asymmetric GaAs n-type double δ-doped quantum wells as a source of intersubband-related nonlinear optical response: effects of an applied electric field, J. Lumin. 147 (2014) 77–84.
[10] A. Keshavarz, M.J. Karimi, Linear and nonlinear intersubband optical absorption in symmetric double semi-parabolic quantum wells, Phys. Lett. 374 (2010) 2675–2680.
[11] M.J. Karimi, A. Keshavarz, Second harmonic generation in asymmetric double semi-parabolic quantum wells: effects of electric and magnetic fields, hydrostatic pressure and temperature, Phys. E Low-dimens. Syst. Nanostruct. 44 (2012) 1900–1904.
[12] E. Ozturk, Nonlinear intersubband transitions in different shaped quantum wells under intense laser field, Superlattice. Microst. 82 (2015) 303–312.
[13] O. Ozturk, E. Ozturk, S. Elagoz, Depending on the intense laser field of the nonlinear optical rectification, second and third harmonic generation in asymmetric parabolic-step and inverse parabolic-step quantum wells, Phys. Scripta 94 (2019) 115809.
[14] H.V. Phuc, L. Van Tung, Linear and nonlinear phonon-assisted cyclotron resonances in parabolic quantum well under the applied electric field, Superlattice. Microst. 71 (2014) 124–133.
[15] M. Sayrac, A. Turkoglu, M.E. Mora-Ramos, F. Ungan, Intensity-dependent nonlinear optical properties in an asymmetric Gaussian potential quantum well-modulated by external fields, Opt. Quant. Electron. 53 (2021) 485.
[16] E.C. Niculescu, L.M. Burileanu, A. Radu, Density of impurity states of shallow donors in a quantum well under intense laser field, Superlattice. Microst. 44 (2008) 173–182.
[17] R.L. Restrepo, J.P. González-Pereira, E. Kasapoglu, A.L. Morales, C.A. Duque, Linear and nonlinear optical properties in the terahertz regime for multiple-step quantum wells under intense laser field: electric and magnetic field effects, Opt. Mater. 86 (2018) 590–599.
[18] M.J. Karimi, H. Vafaei, Second-order nonlinear optical properties in a strained InGaN/AlGaN quantum well under the intense laser field, Superlattice. Microst. 78 (2015) 1–11.
[19] V.V. Tai, N.Q. Khanh, Transport properties of the two-dimensional electron gas in wide AlP quantum wells including temperature and correlation effects, Phys. E Low-dimens. Syst. Nanostruct. 67 (2015) 84–88.
[20] H.S. Li, Y.W. Chen, K.L. Wang, D.Y.C. Lie, Intersubband transitions in pseudomorphic InGaAs/GaAs/AlGaAs multiple step quantum wells, J. Vac. Sci. Technol. B 11 (1993) 1840–1843.
[21] İ. Karabulut, H. Şafak, Nonlinear optical rectification in semiparabolic quantum wells with an applied electric field, Phys. B Condens. Matter 368 (2005) 82–87.
[22] L. Zhang, Electric field effect on the linear and nonlinear intersubband refractive index changes in asymmetrical semiparabolic and symmetrical parabolic quantum wells, Superlattice. Microst. 37 (2005) 261–272.
[23] S. Baskoutas, C. Garoufalis, A.F. Terzis, Linear and nonlinear optical absorption coefficients in inverse parabolic quantum wells under static external electric field, Eur. Phys. J. B 84 (2011) 241–247.
[24] O. Ozturk, B.O. Alaydin, D. Altun, E. Ozturk, Intense laser field effect on the nonlinear optical properties of triple quantum wells consisting of parabolic and inverse-parabolic quantum wells, Laser Phys. 32 (2022), 35404.
[25] B.O. Alaydin, Effect of high bandgap AlAs quantum barrier on electronic and optical properties of In0.70Ga0.30As/Al0.60In0.40As superlattice under applied electric field for laser and detector applications, Int. J. Mod. Phys. B 35 (2021) 2150027.
[26] B.Ö. Alaydin, Optical properties of GaAs/$Al_xGa_{1-x}As$ superlattice under E-field for quantum cascade laser application, Gazi University Journal of Science 34 (2021) 1179–1191.
[27] L. Ajili, G. Scalari, N. Hoyler, M. Giovannini, J. Faist, InGaAs–AlInAs/InP terahertz quantum cascade laser, 87, 2005, p. 141107.
[28] V. Donchev, K. Germanova, N. Shtinkov, I. Ivanov, S. Vlaev, Photoluminescence study of AlAs/GaAs superlattices containing enlarged wells, Thin Solid Films 364 (2000) 224–227.
[29] F. Janiak, M. Dyksik, M. Motyka, K. Ryczko, J. Misiewicz, K. Kosiel, M. Bugajski, Advanced optical characterization of AlGaAs/GaAs superlattices for active regions in quantum cascade lasers, Opt. Quant. Electron. 47 (2015) 945–952.
[30] K. Nakamura, A. Shimizu, M. Koshiba, K. Hayata, Finite-element analysis of quantum wells of arbitrary semiconductors with arbitrary potential profiles, IEEE J. Quant. Electron. 25 (1989) 889–895.
[31] E. Ozturk, Nonlinear optical absorption in graded quantum wells modulated by electric field and intense laser field, Eur. Phys. J. B 75 (2010) 197–203.
[32] I. Altuntas, H. Dakhlaoui, M.E. Mora-Ramos, F. Ungan, Combined effects of electric, magnetic, and intense terahertz laser fields on the nonlinear optical properties in GaAs/GaAlAs quantum well with exponentially confinement potential, European Phys. J. Plus 136 (2021) 1174.
[33] Z.-H. Zhang, J.-H. Yuan, K.-X. Guo, The combined influence of hydrostatic pressure and temperature on nonlinear optical properties of GaAs/Ga0.7Al0.3As morse quantum well in the presence of an applied magnetic field, Materials 11 (2018) 668.